DEFORMABLE MULTI-SCALE SCHEME FOR BIOMETRIC PERSONAL IDENTIFICATION

Gaurav Jaswal, Ravinder Nath

Department of Electrical Engineering
National Institute of Technology Hamirpur
Hamirpur-177005

Aditya Nigam

School of Computing and Electrical Engineering
Indian Institute of Technology Mandi
Mandi-175005

ABSTRACT

Human identification has now been a social liability due to frequent terror threats and corrupt bureaucratic practices, especially in rural countries like India. It has been surprisingly observed that fingerprint quality is poor as compared with finger knuckle quality of rural users as they exist on the outer hand side. In this paper, we are proposing a novel finger-knuckle-print based identification system. Initially, finger knuckle image is pre-processed using proposed local and adaptive image transformations. Then, finger knuckle image matching has been performed using multi-scale Deep-Matching technique. Finally, score level fusion rule has been employed to achieve competitive performance over public FKP database.

1. INTRODUCTION

In the present scenario, hand based biometric traits have been intensively studied to develop a consistent human identification system with higher precision, usability and acceptance. Hand biometric traits such as palm print [21], finger knuckle print (FKP) [8], Hand Geometry [11] etc. have very unique anatomical structures that can be captured using low cost devices. In several Asian countries like India more than 60% of the population reside in rural areas. It has been observed that the quality of their fingerprint is not very good. The laborers, cultivators do substantial work and use their hands very roughly causing permanent damage to their fingerprint. But quality of FKP remains unaffected because they can not be used for any other purpose and hence less prone to injuries [10]. The convex shape skin patterns formed on finger dorsal surface specifically at Proximal Inter Phalangeal (PIP) finger joint are termed as finger knuckle print (FKP) [7]. They contain rich skin patterns, creases and are believed to be very unique, universal, and permanent among individuals [3]. They lie on outer side of finger hence survive longer. Its user failure to enroll (FTE) rate is lower (in rural environment) then fingerprint. Moreover, the dorsal knuckle patterns cannot be easily duplicated and the possibility of information loss from this region is also very less.

Personal identification using finger knuckle features had been proposed in early 90's [4]. Subsequently, continuous efforts were made in this area. In [17], 2-D Gabor filter was employed to extract local orientation information. In [12] radon transform has been applied on enhanced knuckle images that resulted in 1.14% EER and 98.6% CRR. In [18], the phase and orientation information from knuckle images was computed. Likewise in [19], authors combined the magnitude and orientation information. In [20], the authors used a weighted sum rule to fuse local and global information to achieve optimum results. In [14], SIFT key points from Gabor filter based enhanced FKP images were extracted. In [3], knuckle texture had been used as an identifier for smart-phone applications. In [9], the authors performed matching over recovered knuckle minutiae samples. However, there exist a big challenge to track the middle knuckle line for FKP registration because there might be deviations in spatial location of fingers during acquisition. It has been observed that local descriptors (such as SIFT [13] and SURF [2]) focus at salient locations but fails to match deformable regions. To handle such non-rigid deformation and displacement, we have proposed a deformable multi-scale scheme for personal identification using local transformations and Deep-matching [16].

2. PROPOSED APPROACH

Initially, FKP region near Proximal Inter Phalangeal joint (PIP) has been extracted using a ROI extraction algorithm [15] and then ROI is processed further using following steps.

[a] Enhancement : Sample is partitioned into non overlapping cells (10×10) and estimated illumination has been divided (assumed multiplicative noise) from corresponding cell to obtain uniformly illuminated sample. Then its enriched using CLAHE, with noise reduction using Wiener filtering as depicted in Fig 1(e).

(a) I_{ROI} (b) Steady (c) En.(Add.) (d) En.(Mul.) (e) Denoised

Fig. 1. Enhancement : Additive 1(c) Vs Multiplicative 1(d)

[a] FKP ROI Transformation : Sample is encoded using a novel transformation viz. Bubble Ordinal Pattern (BOP) and Star Ordinal Pattern (SOP) as also shown in Fig. 3. They provide a transverse and longitudinal representations robust to lighting conditions and forms a basis using characteristics of edge maps instead of gray values. Further, ray tracing has been used to detect tabular knuckle features.

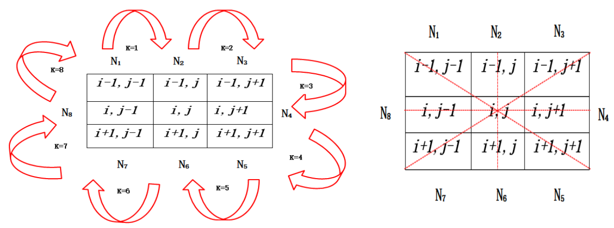

(a) BOP Pattern (b) SOP Pattern

Fig. 2. Neighborhood pattern used for image transformation

[a.1] Bubble Ordinal Pattern (BOP) : The computational steps related to BOP are mentioned in Algorithm 1. The opted Sobel kernel (9×9) can estimate thick and discriminative edges. The proposed scheme uses Sobel longitudinal kernel to assign a 8-bit code (l_{BOP}) for every pixel by comparing its derivatives with 8 of its neighbors, as shown in Fig. 2(a). The BOP_{Code} response for each pixel is a 8-bit binary

Algorithm 1 BOP Algorithm

Require:
The image gradient (I_g) of size $w \times h$.
Ensure:
Encoded images I_{BOP} of size $(w-2) \times (h-2)$.

```
1: for u,v=1 to (w-1),(h-1) do
2:     for k=1 to 8 do
3:         if G_k > G_{(k+1)%8} then
4:             BOP(u,v)[k] = 1
5:         else
6:             BOP(u,v)[k] = 0
7:         end if
8:     end for
9: end for
```

number whose k^{th} bit is stipulated in Eq. 1:

$$BOP_{Code}(u,v)[k] = (G_K > G_{k+1}) \,?\, 1 \;:\; 0 \tag{1}$$

where, $G_K, \forall K \in 1,2,3....8$ represent gradients of eight adjoining pixels around u, v using transverse or longitudinal Sobel kernels. Therefore, l_{BOP} or t_{BOP} are BOP_{Code} based representation of all pixels in a ROI and computed in step 2 of Algorithm 1. It has been observed that transverse derivatives are variable but longitudinal FKP features are prominent hence we have dropped transverse (t_{BOP}).

[a.2] STAR Ordinal Pattern (SOP) : Gradient of any pixel can be $+ve$, $-ve$ or 0 based on its edge position. A 8 bit ordinal encoding has been computed for every pixel, using its diagonally opposite neighbors (as shown in Fig. 2(b)) to get SOP_{Code}, using the Algorithm 2 as shown in Figs. 3(d), 3(e).

Algorithm 2 SOP Algorithm

Require:
The image gradient (I_g) of size $w \times h$.
Ensure:
Encoded images I_{SOP} of size $(w-2) \times (h-2)$.

```
for u,v=1 to (w-1),(h-1) do
    i=1;k=1
    while k < 8 do
        if G_i > G_{(i+4)%8} then
            SOP(u,v)[k] = SOP(u,v)[k+1] = 1
        else
            SOP(u,v)[k] = SOP(u,v)[k+1] = 0
        end if
        i=i+1;k=k+2
    end while
end for
```

[a.3] Image Ray Transform (IRT) : In this work, IRT [5] has been used for the first time to best of our knowledge to emphasize the curved features from transformed FKP images as shown in Fig. 3. The transform treats an image pixels as a set of 2-D glass blocks with refractive indices linked to intensity of pixel and then operate by casting a large number of rays through the image. These ray interactions are accumulated into output image which then emphasize FKP tabular features. Given any transformed knuckle image (I_T) of size $(m \times n)$, a refractive index (n_i) value for the i^{th} pixel has been computed as a linear function of its respective gray intensity.

$$n_i = 1 + (\frac{g}{255})(n_{max} - 1) \tag{2}$$

whereas, n_{max} represents the max. refractive index. While ray tracing the θ_i (angle of incidence) and θ_r (angle of reflection) can be calculated as:

$$\cos\theta_i = N.V; n = \frac{n_1}{n_2}; \cos\theta_r = \sqrt{1 - n^2(1 - N.V)} \tag{3}$$

where, N is normal direction and V is a vector function of the initial direction at each pixel. Hence refraction and reflection vector (if $\theta_i > \theta_c$ and $n_1 > n_2$), for pixels of different refractive index, can be given as:

$$R_r = nV + (n(N.V) - \cos\theta_r)N; R_l = V - 2(N.V)N \tag{4}$$

At an initial randomly chosen direction ϕ, a ray starts from a pixel. The overall methodology is outlined in Algorithm 3 and parametric descriptions are given in Table 1.

[b] Deep-Matching based Identification : The SIFT feature fails to match non-rigid deformable region [16], because 4 patches in SIFT were rigid and unable to account non-linear deformations. A dense matching algorithm for non-rigid objects has been employed called as Deep-Matching [16], which is a multi-stage architecture with 6 layers inspired from deep convolution nets but do not learn any representation.The SIFT/SURF/HOG descriptors match 4×4 sized patches between two images by generating a real $d = 128$ dimensional vector in space $V \in \Re^{d=4\times4\times8}$. In

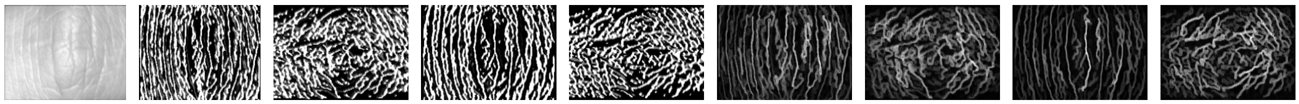

(a) I_R (b) l_{BOP} (c) t_{BOP} (d) l_{SOP} (e) t_{SOP} (f) KCP_{lBOP} (g) KCP_{tBOP} (h) KCP_{lSOP} (i) KCP_{tSOP}

Fig. 3. Image Transfor. and Encoding Schemes using BOP, SOP followed by IRT (Transverse components are discarded)

Algorithm 3 Steps involved in IRT Algorithm

Require:
Encoded FKP image l_{BOP}, l_{SOP} of size $w \times h$.
Ensure:
Segmented image KCP_{lBOP}, KCP_{lSOP} of $w \times h$ size

```
Initi. N random pts. and φ directions from 𝒩 and define refractive index n_i, for any i^th pixel using equation 2.
Direction and incidence angles are denoted as X_i, φ_i for any θ_i ∀i ∈ {1, 2, 3, ..., N}
Initialize depth=1 //(max.dept = d)
for i=1:N do
    while depth < d do
        if (θ_i < θ_c)||(n_i < n_{i+1})||(n_i > n_{i+1}) then
            Refraction occurs with vector R_r
        else if θ_i > θ_c then
            Reflection occurs with vector R_l
        end if
        depth = depth + 1
    end while
end for
```

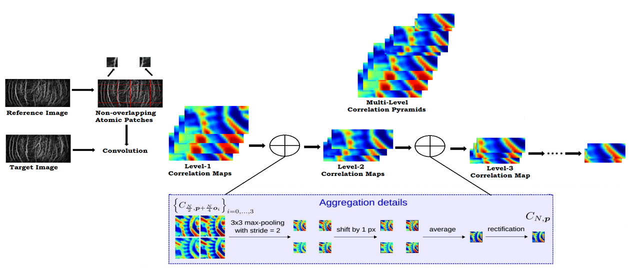

Fig. 4. Corr. Maps:Ref. matched to Tar. via. DeepMatching

Deep-matching SIFT patch has been split into 4 quadrants represented as $I = [I^0, I^1, I^2, I^3]$ such that $I^n \in \Re^{2\times2\times8}$. Now while matching reference patch with target patch, target descriptor of the quadrants of size 4×4 grid have not been kept fixed. Actually their positions are obtained by maximizing $Sim(I, I'(p)) = \frac{1}{4}\sum_{i=0}^{3} \max_{p_i} sim(I_i, I'(p_i))$, where $I'(p) \in \Re^{2\times2\times8}$ is the descriptor of a single quadrant extracted at position p. Such similarity can be estimated efficiently with the assumption that each of these quadrants can move independently to get a coarse non-rigid matching score. This method can perform reasonable non-rigid matching with explicit pixel-wise correspondences, if it is applied in recursive nature. For example, two given images I_R and I_T are compared using algorithm 4. The matching algorithm is divided into two main steps: (1) Correlation maps are computed using a bottom-up algorithm which include convolution, max-pooling and sub-sampling as depicted in Fig 4. (2) Top-down method estimates the motion of atomic patches starting from top level correlation maps as shown in Fig. 5.

Algorithm 4 Deep-Matching

Require:
Reference I_R and Target I_T sample sized $m \times n$.
Ensure: Similarity score between given two images.

1. Divide I_R into atomic patches of size 4×4 pixels and compute correlation map $C_{4,p} = I_{R(4,p)} * I_T$ between each atomic patch in I_R and whole I_T recursively, where p= N > 4, is a power of 2.
2. Aggregate correlation maps of four $\frac{N}{2} \times \frac{N}{2}$ sized atomic patches to create a $N \times N$ size larger patch and perform max-pooling at each level by sliding 3×3 sized grid.
3. Perform sub-sampling and apply non-linear mapping function (γ rectification) to extend range of correlation values at each level. Then compute multilevel correlation pyramid $(C_{N,p})_{N,p}$ representing average similarity score between two images.
4. Lastly perform backtracking for undoing aggregation so as to recover corresponding matching points of atomic-patches at lower level. Finally extract local maxima (M_1) from each correlation map at each level and then find the next local maxima (M_2) in the neighbourhood of M_1.

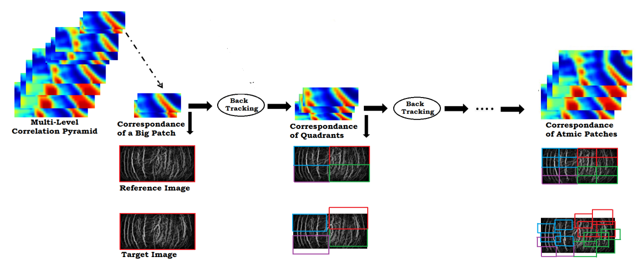

Fig. 5. Top down correspondence over Corr. map pyramid

Table 1. Description of Parameters

Parameter	Range	Description	Nature
		CLAHE	
f_{scale}	0.4-0.6	Scaling down	Moderate
$Block\ Size$	10×10	Blocking size	Low
		BOP/SOP	
$Sobel\ Kernel$	9×9	Block size for gradient	High
		Image Ray Transform	
n_{max}	100	Max. refractive index	Low
$depth(d)$	256	ray tracing depth (d)	High
N	10000	points for experiment	High
		DeepMatching	
$Patch\ Size$	4×4	Atomic Patch size	Low
$Maxpooling$	3×3	Max-pool with stride = 2	Low
$Rectification$	1.4	γ corr. power factor	Moderate
$Rotation$	-/+26°	Rotational Invariance	High

3. EXPERIMENTAL RESULTS

The benchmark publicly available, PolyU FKP dataset [1] has been used for performance evaluation containing 7920 images. We have generated a small validation data set consist of 50 subjects by considering first 20 subjects from each finger LI, LM, RI, RM. he best performing parametric set

Table 2. Comparative Analysis (Results as reported in [6] with exactly same testing protocol)

	Full FKP db		Left Index		Left Middle		Right Index		Right Middle	
Algorithm	EER	(%)CRR	EER	(%)CRR	EER	(%)CRR	EER	(%)CRR	EER	(%)CRR
Compcode [17]	1.386	-	1.884	-	1.883	-	1.445	-	1.175	-
BOCV [21]	1.833	-	2.202	-	2.299	-	1.892	-	1.647	-
ImCompcode+MagCode[20]	1.210	-	1.610	-	1.650	-	1.326	-	1.097	-
MoriCode [6]	1.201	-	1.544	-	1.698	-	1.605	-	1.244	-
MtexCode [6]	1.816	-	2.077	-	2.078	-	2.115	-	2.055	-
MoriCode and MtexCode [6]	1.0481	-	1.328	-	1.453	-	1.247	-	1.063	-
Deep-Matching l_{BOP}	7.35	96.45	8.84	96.36	6.97	96.86	8.71	94.64	7.38	99.56
Deep-Matching KCP_{lBOP}	3.13	98.81	4.12	98.68	3.66	99.29	3.17	99.09	3.44	99.69
Deep-Matching l_{SOP}	2.93	98.86	3.42	98.78	2.96	99.39	3.57	99.59	3.64	99.29
Deep-Matching KCP_{lSOP}	1.93	99.62	2.50	99.39	1.74	100	1.84	100	1.99	99.39
Deep-Matching Proposed Fusion	**0.92**	99.39	**1.10**	99.39	**0.96**	100	**0.98**	100	**0.97**	99.79

has been chosen in terms of CRR and EER. Detailed parametric description has been presented in Table 1.

ROC based Analysis : Performance metrics used for analysis are Equal Error Rate(EER), Correct Recognition Rate (CRR), Error under ROC Curve EUC, and Decidability Index (DI). We have performed inter-session matching by using first 6 images as gallery and remaining as probe.

Test 1: In first experiment, four categories of PolyU FKP database: Right Index (RI), Right Middle (RM), Left Index (LI), Left Middle (LM) are considered independently. Based on testing protocol of our system, total of $(165*6)*6 = 5,940$ genuine and $(165 * 6) * (164 * 6) = 9,74,160$ impostor matches are reported. The KCP_{lBOP} based schemes gave significant improvement in results over KCP_{lSOP} transformation because FKP image patterns are better justified in BOP based longitudinal gradient. The multi-feature fusion outperforms individual feature based schemes while one can also observe that the optimum EER of 0.96% and CRR of 100% are achieved with LM images as mentioned in Table 3.

Table 3. ROC based Performance Analysis

Description	DI	EER(%)	Accuracy(%)	EUC	CRR(%)
Left Index finger-knuckle-print PolyU Database					
$fusion$	3.40	1.10	98.722	0.261	99.39
Left Middle finger-knuckle-print PolyU Database					
$fusion$	3.44	0.96	99.015	0.094	100
Right Index finger-knuckle-print PolyU Database					
$fusion$	3.51	0.98	99.151	0.145	100
Right Middle finger-knuckle-print PolyU Database					
$fusion$	3.51	0.97	98.97	0.149	99.79
Full FKP finger-knuckle-print PolyU Database					
l_{BOP}	2.32	3.13	97.088	0.8323	98.81
KCP_{lBOP}	2.36	1.93	98.42	0.339	99.62
l_{SOP}	1.911	7.35	93.18	3.366	96.45
KCP_{lSOP}	2.268	2.93	97.393	0.789	98.86
$fusion$	3.304	0.92	99.061	0.1414	99.39

Test 2: In the second test, all subjects (660) and their corresponding poses $(660 * 12)$ are included for performance evaluation. Thus, a total number of $15,657,840$ impostor and $23,760$ genuine matching scores are computed. The results for complete FKP data set are described in Table 3 and ROC plots are shown in Fig. 6(a). The proposed multi feature fusion scheme achieves 0.92 % EER over full FKP dataset which is significantly higher than four individual feature based schemes. The genuine Vs impostor score distribution has been presented in Fig. 6(b) for fusion scheme over full FKP database. A well discriminating characteristic can be observed, as also reported in terms of discriminating index ($DI = 3.304$) in Table 3.

Comparative Analysis : The performance of proposed system has been compared against some well-known systems as shown in Table 2. One can observe that Compcode [17] and fusion of MoriCode and MtexCode [6] has been performing consistently well. But the proposed scheme has achieved superior performance. Fusion of multiple features as reported in [6] and [20] has also been surpassed by our proposed fusion.

4. CONCLUSION

We have proposed a system that can be suitable to enable financial inclusion of rural community, based on score level fusion of multiple FKP features. Samples are transformed using novel BOP, SOP, IRT schemes to obtain robust image representations and are matched using a hierarchical Deep-matching. The PolyU FKP benchmark data-set has been used for performance evaluation and as compared with other state of art methods have achieved superior results.

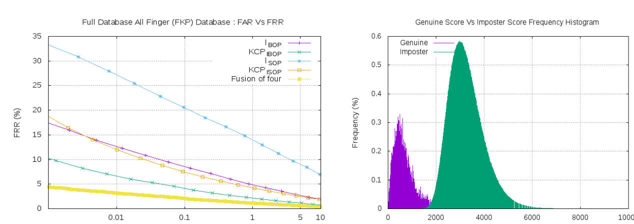

(a) ROC for full FKP database (b) Gen. Vs Imp. Score Distr.

Fig. 6. Test 2 - Performance analysis (Full FKP)

5. REFERENCES

[1] Finger-knuckle-print polyu. `http://www.comp.polyu.edu.hk/biometrics`, 2009.

[2] H. Bay, A. Ess, T. Tuytelaars, and L. Van Gool. Speeded-up robust features (surf). *Computer vision and image understanding*, 110(3):346–359, 2008.

[3] K. Cheng and A. Kumar. Contactless finger knuckle identification using smartphones. In *Proceedings of the International Conference of the Biometrics Special Interest Group*, pages 1–6. IEEE, 2012.

[4] C. Colbert. Knuckle profile indentity verification system, Jan. 14 1997. US Patent 5,594,806.

[5] A. H. Cummings, M. S. Nixon, and J. N. Carter. The image ray transform for structural feature detection. *Pattern Recognition Letters*, 32(15):2053–2060, 2011.

[6] G. Gao, J. Yang, J. Qian, and L. Zhang. Integration of multiple orientation and texture information for finger-knuckle-print verification. *Neurocomputing*, 135:180–191, 2014.

[7] T. Kong, G. Yang, and L. Yang. A new finger-knuckle-print roi extraction method based on probabilistic region growing algorithm. *International Journal of Machine Learning and Cybernetics*, 5(4):569–578, 2014.

[8] A. Kumar. Importance of being unique from finger dorsal patterns: Exploring minor finger knuckle patterns in verifying human identities. *IEEE Transactions on Information Forensics and Security*, 9(8):1288–1298, 2014.

[9] A. Kumar and B. Wang. Recovering and matching minutiae patterns from finger knuckle images. *Pattern Recognition Letters*, 68:361–367, 2015.

[10] A. Kumar and Z. Xu. Personal identification using minor knuckle patterns from palm dorsal surface. *IEEE Transactions on Information Forensics and Security*, 11(10):2338–2348, 2016.

[11] A. Kumar and D. Zhang. Hand-geometry recognition using entropy-based discretization. *IEEE Transactions on information forensics and security*, 2(2):181–187, 2007.

[12] A. Kumar and Y. Zhou. Human identification using knucklecodes. In *IEEE 3rd International Conference on Biometrics: Theory, Applications, and Systems*, pages 1–6. IEEE, 2009.

[13] D. G. Lowe. Distinctive image features from scale-invariant keypoints. *International journal of computer vision*, 60(2):91–110, 2004.

[14] A. Morales, C. Travieso, M. Ferrer, and J. Alonso. Improved finger-knuckle-print authentication based on orientation enhancement. *Electronics Letters*, 47(6):380–381, 2011.

[15] A. Nigam and P. Gupta. Finger-knuckle-print roi extraction using curvature gabor filter for human authentication. In *Proceedings of the 11th Joint Conference on Computer Vision, Imaging and Computer Graphics Theory and Applications*, pages 364–371, 2016.

[16] J. Revaud, P. Weinzaepfel, Z. Harchaoui, and C. Schmid. Deepmatching: Hierarchical deformable dense matching. *International Journal of Computer Vision*, pages 1–24, 2015.

[17] L. Zhang, L. Zhang, and D. Zhang. Finger-knuckle-print: a new biometric identifier. In *16th IEEE International Conference on Image Processing*, pages 1981–1984. IEEE, 2009.

[18] L. Zhang, L. Zhang, and D. Zhang. Monogeniccode: A novel fast feature coding algorithm with applications to finger-knuckle-print recognition. In *International Workshop on Emerging Techniques and Challenges for Hand-Based Biometrics*, pages 1–4. IEEE, 2010.

[19] L. Zhang, L. Zhang, D. Zhang, and H. Zhu. Online finger-knuckle-print verification for personal authentication. *Pattern recognition*, 43(7):2560–2571, 2010.

[20] L. Zhang, L. Zhang, D. Zhang, and H. Zhu. Ensemble of local and global information for finger-knuckle-print recognition. *Pattern Recognition*, 44(9):1990 – 1998, 2011.

[21] Q. Zheng, A. Kumar, and G. Pan. Suspecting less and doing better: New insights on palmprint identification for faster and more accurate matching. *IEEE Transactions on Information Forensics and Security*, 11(3):633–641, 2016.